



Cite this: *Nanoscale*, 2016, **8**, 16259

## Strong dichroic emission in the pseudo one dimensional material $ZrS_3$ †

Anupum Pant,<sup>a</sup> Engin Torun,<sup>b</sup> Bin Chen,<sup>a</sup> Soumya Bhat,<sup>a</sup> Xi Fan,<sup>a</sup> Kedi Wu,<sup>a</sup> David P. Wright,<sup>c</sup> Francois M. Peeters,<sup>b</sup> Emmanuel Soignard,<sup>c</sup> Hasan Sahin<sup>d</sup> and Sefaattin Tongay<sup>\*a</sup>

Zirconium trisulphide ( $ZrS_3$ ), a member of the layered transition metal trichalcogenides (TMTCs) family, has been studied by angle-resolved photoluminescence spectroscopy (ARPLS). The synthesized  $ZrS_3$  layers possess a pseudo one-dimensional nature where each layer consists of  $ZrS_3$  chains extending along the *b*-lattice direction. Our results show that the optical properties of few-layered  $ZrS_3$  are highly anisotropic as evidenced by large PL intensity variation with the polarization direction. Light is efficiently absorbed when the E-field is polarized along the chain (*b*-axis), but the field is greatly attenuated and absorption is reduced when it is polarized vertical to the 1D-like chains as the wavelength of the exciting light is much longer than the width of each 1D chain. The observed PL variation with polarization is similar to that of conventional 1D materials, *i.e.*, nanowires, and nanotubes, except for the fact that here the 1D chains interact with each other giving rise to a unique linear dichroism response that falls between the 2D (planar) and 1D (chain) limit. These results not only mark the very first demonstration of PL polarization anisotropy in 2D systems, but also provide novel insight into how the interaction between adjacent 1D-like chains and the 2D nature of each layer influences the overall optical anisotropy of pseudo-1D materials. Results are anticipated to have an impact on optical technologies such as polarized detectors, near-field imaging, communication systems, and bio-applications relying on the generation and detection of polarized light.

Received 1st July 2016,  
Accepted 8th August 2016

DOI: 10.1039/c6nr05238j

www.rsc.org/nanoscale

## Introduction

Lamellar materials consist of individual 2D sheets where weak vdW interactions play an important role. Most of these layered materials are rather uniform/isotropic in the *ab*-plane but appear structurally decoupled along the *c*-axis. After the experimental demonstration of semi-metallic graphene<sup>1–3</sup> and direct gap semiconductor  $MoS_2$ <sup>4</sup> by exfoliation from graphite and molybdenite lamellar crystals, layered materials have gained enormous interest due to their unique properties when scaled down from bulk to monolayer. Examples include transition metal dichalcogenides (TMDCs) with  $MX_2$ <sup>5–7</sup> and post-transition metal chalcogenides (PTMCs) with the<sup>8–10</sup> general chemical

formula  $MX$  where M stands for transition or post-transition metal atoms and X is the chalcogen group (S, Se, and Te). With the exception of the V-TMDC group, such as  $ReS_2$  and  $ReSe_2$ ,<sup>11,12</sup> TMDCs materials possess rather uniform properties within the plane perpendicular to the *c*-axis (*ab*-plane).

However, there exist a small number of materials with strong in-plane structural anisotropy. Some examples of these materials are black phosphorus,<sup>7,13,14</sup> group-V TMDCs ( $ReS_2$  and  $ReSe_2$ ),<sup>11,12</sup> and transition metal trichalcogenides ( $MX_3$ ).<sup>15–19</sup> These materials differ from isotropic layered materials in that each individual layer consists of a superlattice of 1D chains extending along one particular lattice direction. Considering in-plane structural anisotropy, angle dependent Raman measurements have been performed to determine the crystal lattice direction of BPs,  $ReS_2$ , and  $ReSe_2$ . Moreover, theoretical and experimental studies have shown that  $MX_3$ <sup>15,20</sup> and BP flakes have anisotropic electronic mobility, particularly high electronic mobility along the chain direction.<sup>7,13,14,21</sup> More recently, the Raman/PL spectrum, and polarized photodetector applications have been investigated in  $ReS_2$  and black phosphorus.<sup>11,12,22–24,42</sup>

Despite these pioneering studies, our understanding of pseudo-1D materials, particularly TMTCs with the chemical

<sup>a</sup>School for Engineering of Matter, Transport and Energy, Arizona State University, Tempe, Arizona 85287, USA. E-mail: Sefaattin.tongay@asu.edu

<sup>b</sup>Department of Physics, University of Antwerp, Groenenborgerlaan 171, B-2020 Antwerp, Belgium

<sup>c</sup>LeRoy Eyring Center for Solid State Science, Arizona State University, Tempe, Arizona 85287, USA

<sup>d</sup>Department of Photonics, Izmir Institute of Technology, Izmir 35430, Turkey

†Electronic supplementary information (ESI) available. See DOI: 10.1039/c6nr05238j

formula  $\text{MX}_3$  ( $\text{M} = \text{Zr}, \text{Ti}, \text{Hf}$  and  $\text{X} = \text{S}, \text{Se}, \text{and Te}$ ), is still in its infancy. TMTCs are a new class of layered materials with strong in-plane anisotropy. Each TMTC layer consists of 1D chains made of an  $\text{MX}_6$  polyhedron extending along the  $b$ -direction.<sup>25</sup> TMTCs differ themselves from other pseudo-1D materials in that unlike aforementioned anisotropic materials, they are rather luminescent (nearly  $\sim 5$  and  $10$  times more luminescent compared to BPs and  $\text{ReS}_2$  crystals of the same thickness respectively) allowing us to investigate the polarization effects in light emission properties, and stronger in-plane anisotropy due to the formation of weakly coupled  $\text{MX}_6$  1D chains. Due to their reduced crystal symmetry and anisotropy, TMTCs appear needle like as shown in Fig. 1, whereas other in-plane anisotropic systems ( $\text{ReS}_2$  and black phosphorus) appear more planar (2D-like).<sup>7,12</sup> Their needle like structure indirectly implies that the interaction between adjacent chains are potentially weaker compared to other anisotropic systems, and thus anisotropy effects are anticipated to be much stronger.

Optical studies on the pseudo-1D material  $\text{ZrS}_3$  are possible as it strongly emits light in the visible spectrum, it has a rather strong in-plane structural anisotropy due to weak chain-chain interactions, and its environmental stability allows for careful optical spectroscopy measurements without any concern over structural damage as in black phosphorus. The synthesized  $\text{ZrS}_3$  sheets have strong light emission at  $1.8$  eV allowing us to link structural anisotropy to the light emission characteristics

of the pseudo-1D materials for the first time. Angle resolved PL spectroscopy (ARPLS) studies reveal that the maximum integrated PL intensity occurs only when the  $E$ -polarization field is oriented along the chain ( $b$ -) axis direction, whereas the intensity drops by an order of magnitude when the  $E$ -field polarized across the chain direction ( $a$ -axis) after the  $E$ -field is attenuated in the perpendicular direction due to the size effects of 1D like chains in  $\text{ZrS}_3$ . Similar measurements on a large number of few-layered flakes show that polarization anisotropy ( $\rho$  ratio between maxima and minima of the integrated PL intensity) spans from  $5.7$  to  $10.8$ . Interestingly,  $\text{ZrS}_3$ 's optical spectral response appears comparable to truly 1D materials (nanotubes and nanowires), yet polarization anisotropy is always smaller.<sup>26,27</sup> Overall results are understood by our model based on electromagnetic theory which accounts for the deviation from truly 1D behavior by accounting for chain-chain interactions in a pseudo-1D  $\text{ZrS}_3$  system, and thus presents a unique material system with optical properties that fall between the 2D and 1D limit.

## Results and discussion

A tilted side view with a ball and stick representation of  $\text{ZrS}_3$  is shown in Fig. 1a. With blue polyhedrons as guides, it can be seen that  $\text{ZrS}_6$  trigonal prisms sharing triangular faces extend along the  $b$ -axis forming pseudo-1D chain-like structures.

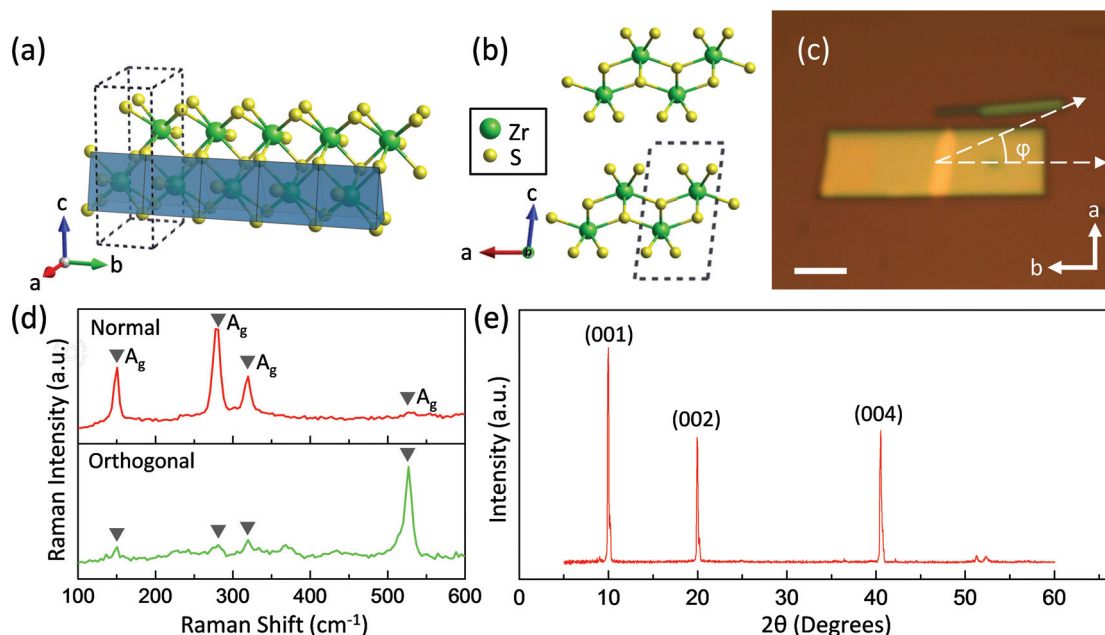


**Fig. 1** (a) Tilted side view of a ball and stick model of a single layer of  $\text{ZrS}_3$ . Zr and S atoms are denoted by green and yellow spheres, respectively. The dotted black line represents the primitive monoclinic cell. And the blue trigonal prisms represent the chain. (b) Stacked layers of bulk  $\text{ZrS}_3$  as seen from the  $b$  axis. (c) A thick ( $\sim 50$  nm)  $\text{ZrS}_3$  flake exfoliated on top of  $\text{SiO}_2/\text{Si}$ .  $\varphi$  is the angle through which the flake is rotated to record angle-dependent data. (Scale bar  $15 \mu\text{m}$ ). (d) Raman peaks of  $\text{ZrS}_3$  obtained for ( $\varphi = 0^\circ$ ) using  $488$  nm laser polarized along the  $b$ -axis (labeled as normal – red plot) and along the  $a$ -axis (labeled as orthogonal – green plot). Detection is polarized parallel and perpendicular to the incident  $E$ -field polarization in normal and orthogonal arrangements, respectively. (e) Powder diffraction XRD peaks from macro sized  $\text{ZrS}_3$  crystals mounted with the  $c$ -axis facing up.

A side view image seen from the *b*-axis direction shows individual ZrS<sub>3</sub> monolayers weakly coupled to adjacent layers *via* vdW forces, and the dashed box highlights the unit cell (Fig. 1b). Inside the 1D prismatic chain unit, six atoms of S are equally separated from the metal Zr atom (~2.63 Å), but the S atoms outside of the chain are slightly farther away (~2.75 Å). These results are consistent with earlier structural studies on ZrS<sub>3</sub> by Wieting *et al.*<sup>28</sup> and results in slightly decoupled 1D-chain like structures confined in the *ab*-plane. Due to the structural in-plane anisotropy of ZrS<sub>3</sub>, the flakes cleave easily along the *b*-axis, resulting in needle-like few-layered flakes with a large geometric aspect ratio (*a/b* < 1). Moreover, the synthesized ZrS<sub>3</sub> crystals appear in a layered whisker form extending in length in one direction. In this work, we have performed our measurements on the large areas of exfoliated ZrS<sub>3</sub> flakes (see Fig. 1c) about 10 to 50 nm in thickness to ensure that (1) the flake is uniformly excited with the laser (spot ~1 μm<sup>2</sup>), (2) sufficient PL can be collected (increased material quantity), and (3) laser damage can be avoided (thinner flakes were found to be damaged under low power excitation ~μW) to probe the intrinsic properties of ZrS<sub>3</sub>. In our measurements, the rotation angle was defined as the azimuthal angle ( $\varphi$ ), *i.e.*, the angle between the *b*-axis and E-field direction, as shown in Fig. 1c.

In this work, ZrS<sub>3</sub> crystals were grown using chemical vapor transport (CVT) of constituent elements vacuum sealed in a quartz tube based on an existing growth procedure.<sup>29,30</sup> Zr powder and S powder was mixed at a stoichiometric 1 : 3 ratio, however, extra sulfur (final Zr/S ratio ~1 : 3.05) and a minuscule amount of an I<sub>2</sub> transport agent was added to facilitate vapor transport from the hot to cold zone. Typical growth took place at ~650 °C ( $T_{\text{hot}} = 650$  and  $T_{\text{cold}} = 620$  °C) and the process was complete after 3 days. The crystallinity of the synthesized flakes was confirmed through Raman spectroscopy, consistent with earlier work.<sup>30–32</sup> We observed 4 prominent peaks all corresponding to Ag modes at 150.5 cm<sup>-1</sup>, 277.6 cm<sup>-1</sup>, 319.6 cm<sup>-1</sup> and 527 cm<sup>-1</sup> (Fig. 1d). The ZrS<sub>3</sub> crystal structure was further confirmed by XRD measurement; the observed XRD data matches well with the established ICDD card (00-015-0790) (Fig. 1e), suggesting that ZrS<sub>3</sub> crystallizes in a monoclinic cell *P*2<sub>1</sub>/*m* space group with lattice constants calculated as  $a = 5.123$  Å,  $b = 3.627$  Å,  $c = 8.986$  Å, and  $\beta = 97.15^\circ$ .

Before discussing our main results on dichroism and the 1D-like PL response, considering the fundamental knowledge gap in understanding ZrS<sub>3</sub> light emission characteristics, we first introduce the band structure and provide an explanation for the light emission characteristics of ZrS<sub>3</sub>. HSE06 calculations<sup>33</sup> – which successfully account for the many-body interactions in layered systems predict that ZrS<sub>3</sub> is a 1.88 eV indirect gap semiconductor which absorbs and emits photons relatively weakly. However, the presence of transition metal or chalcogen vacancies is known to enhance the PL intensity either by delocalizing electrons in the momentum space (within the Heisenberg principle if the position of the electron is well defined – trapped location – its momentum is largely

unknown) or by decreasing the Wannier exciton Bohr radius. The former effect was previously observed in GaP:N<sup>34,35</sup> and the latter was reported by various groups on 2D TMDCs.<sup>36–38</sup> The calculated band structure of ZrS<sub>3</sub> in Fig. 2a shows that localized states are created 0.59 eV below the CBM by incorporating chalcogen (S) single vacancies. Thus, two possible transitions may appear: (1) indirect gap luminescence as observed in few-layered (indirect gap semiconductor) MoS<sub>2</sub>, and (2) defect assisted bound exciton emission appearing at 1.88 eV and ~1.3 eV respectively. Theoretically estimated values closely match the experimentally observed PL spectrum where PL peaks are located at 1.8 eV and 1.45 eV, which might be associated with indirect gap emission and bound exciton emission lines. Here, we note that our absorption spectrum measurements (not shown) show that the band edge is located at ~2 eV, which is close to previously reported values.<sup>39</sup> Thus, alternatively, emission at 1.8 eV may be related to the exciton recombination assisted by delocalization in the *k* space (similar to GaP:N systems) while the 1.45 eV peak is still a bound exciton in nature. Further data for the observed PL characteristics are obtained from power dependent PL measurements in Fig. 2b and c: as seen in the red scatter-spline peak area *vs.* excitation power curve in Fig. 2b, the 1.45 eV peak quickly saturates with increasing laser excitation due to the finite density of bound (defect) states saturating the optical transition through this particular recombination channel, consequently PL *vs.* power plots exhibit signature saturating behavior due to bound excitons. The high energy peak at 1.8 eV, however, scales linearly with laser excitation (slope ~0.91) in the log plot (Fig. 2b) without any saturation.<sup>35</sup>

Next, we present our main result as summarized in the contour plot (for orthogonal arrangement) shown in Fig. 3a. Here, we report an angle-dependent photoluminescence (PL) of ZrS<sub>3</sub> crystals. We find that depending on the angle ( $\varphi$ , see Fig. 1c) of the crystal under a polarized incident laser, the photoluminescence is strongly polarized in one particular direction. From the polar plots shown in Fig. 3b and c, it can clearly be seen that when the electric field of the polarized light is aligned along the chain axis (or parallel to the *b*-axis), a maximum PL intensity is observed ( $I_{\parallel}$ ), and this happens at  $\varphi = 90^\circ$  and  $\varphi = 0^\circ$  in orthogonal and normal arrangements, respectively. While a minimum intensity ( $I_{\perp}$ ) is observed when the electric field of the polarized light is perpendicular to the chain direction (or parallel to *a*-axis), this happens at  $\varphi = 0^\circ$  and  $\varphi = 90^\circ$  in orthogonal and normal arrangements, respectively. It is noteworthy that similar measurements on thinner (<10 nm) ZrS<sub>3</sub> flakes (as shown in Fig. 3d) yield similar anisotropic PL responses (*i.e.*, anisotropy ratio and shape) to thicker (~50 nm Fig. 3d) flakes. The atomic force microscopy (AFM) measurements on thin and thick flakes are shown in Fig. S1.† However, measurements on even thinner flakes significantly introduced sample damage, and prevented us from acquiring data on their pristine response.

However, our control studies on direct bandgap MoS<sub>2</sub> monolayers appear completely isotropic (independent from

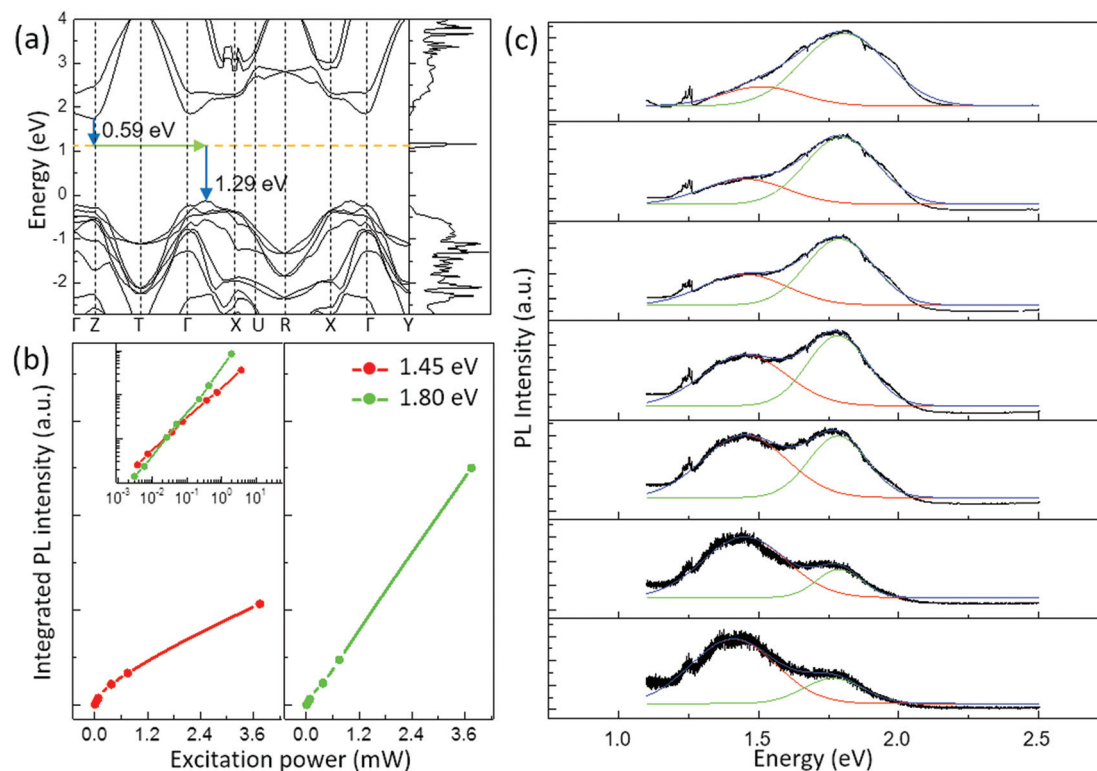


**Fig. 2** (a) Band structure of bulk  $\text{ZrS}_3$  and density of states of bulk  $\text{ZrS}_3$  with S vacancy within HSE06 approximation. (b) A plot of area under the PL peak vs. the laser excitation power. The red curve and green curves are for the 1.45 eV and 1.8 eV peaks respectively. Inset image shows the plots in a log–log scale. (c) The PL spectra at various powers from 0.05%–50% laser excitation power (where 100% power corresponds to 7.5 mW). The red and green curves are Gaussian fits for the 1.45 eV and 1.8 eV peaks, respectively.

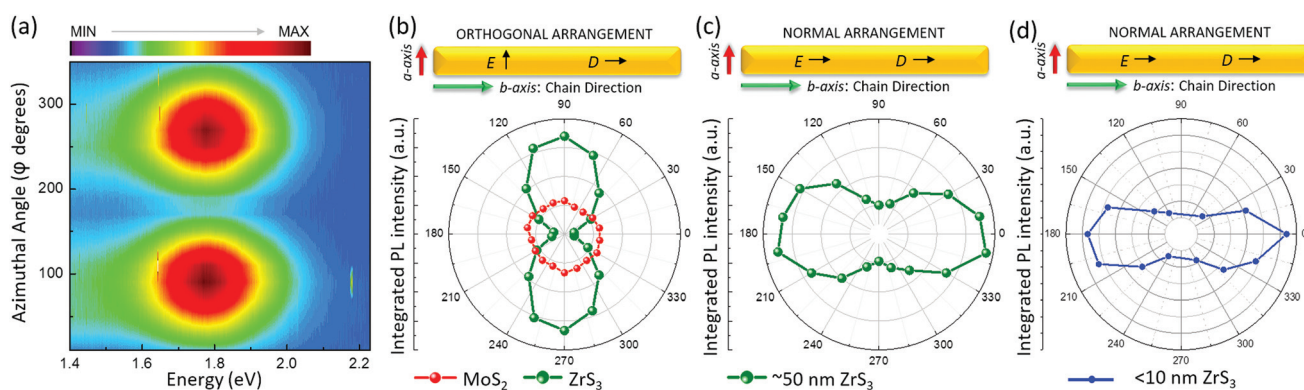


**Fig. 3** (a) A contour plot of the angle dependence of PL on a  $\sim 50$  nm thick  $\text{ZrS}_3$  flake in orthogonal arrangement. (b) Polar plot of the integrated peak area with azimuthal flake angle ( $\varphi$ ) in orthogonal arrangement (c) and in normal arrangement. (See the schematic of arrangements above the respective polar plots;  $E$  is the electric field direction of the polarized excitation laser and  $D$  is the polarization direction of the detector). (d) Polarization dependent PL polar plots taken from  $<10$  nm thick  $\text{ZrS}_3$  nanoflakes.

polarization direction) as shown by red circles in Fig. 3b. Considering the vastly different polarization dependence of  $\text{MoS}_2$  and  $\text{ZrS}_3$ , and along with structural isotropy and anisotropy of  $\text{MoS}_2$  and  $\text{ZrS}_3$ , we attribute this anisotropic optical behavior to the pseudo-1D structure of  $\text{ZrS}_3$ . It is, however, important to note that the polarization dependent PL response of  $\text{ZrS}_3$  flakes significantly differ from those observed in aniso-

tropic black phosphorus.<sup>24</sup> It has been previously shown that excitons are linearly polarized along the light effective mass direction ( $x$ -direction) which is independent of the exciting polarization direction. In contrast, the PL of  $\text{ZrS}_3$  flakes is maximized along the polarization direction possibly due to similar effective mass values (along different crystal directions) preventing the formation of linearly polarized excitons.

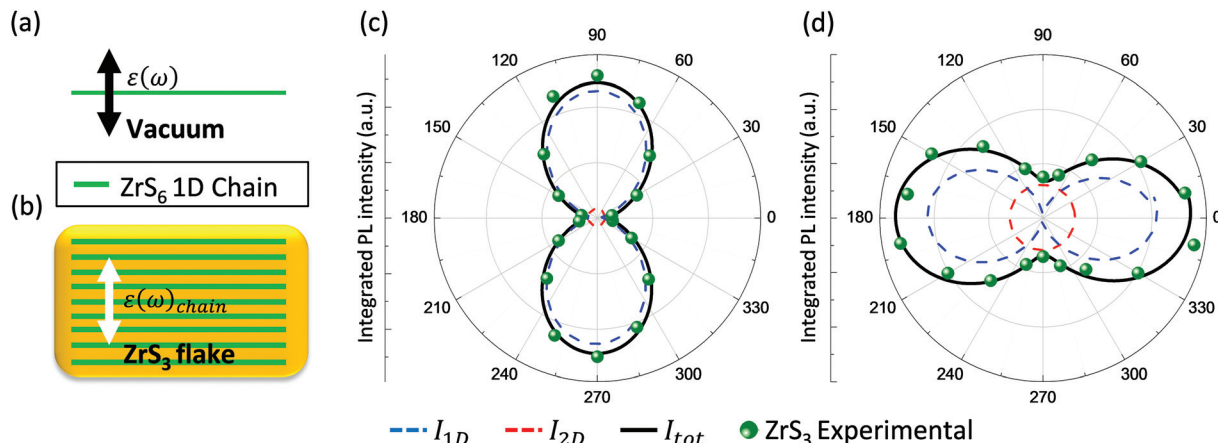


**Fig. 4** (a) A representation of a 1D-chain/nanowire under vacuum with a permittivity contrast of  $\epsilon(\omega)$  (b) A representation of chains inside a  $\text{ZrS}_3$  flake with a far lower permittivity contrast  $\epsilon(\omega)_{\text{chain}}$ . (c) Cosine square fits (black line) of the actual data (green scatter-line), with  $I_{1D}$  and  $I_{2D}$  are shown in blue and red dotted lines respectively, in orthogonal arrangement (d) and in normal arrangement.

Naturally, structural anisotropy is anticipated to influence the properties of materials especially in reduced dimensions. The next question is: what is the origin of polarized PL emission? This effect can be explained by classical electromagnetic theory. Consider a one-dimensional isolated trigonal prismatic chain of  $\text{MX}_3$  running parallel to the  $b$ -axis which acts as a free standing nanowire: the absorption is rather strong when  $E$  is parallel to the chain direction ( $E \parallel b$ ). The electric field inside the flake is not reduced ( $E_{\text{in}\parallel} = E_{\text{out}\parallel}$ ). In contrast, when the electric field of the polarized laser is perpendicular ( $E_{\text{out}\perp}$ ) to the infinite dielectric chains, because the wavelength of the exciting light is much larger than the individual chain width, the electrical field amplitude ( $E_{\text{in}\perp}$ ) inside the wire is greatly attenuated, thus absorption is low. Depending on the permittivity contrast  $\epsilon(\omega)$  between the nanowire and the surrounding medium, this attenuation in the quasi-static limit (for a cylindrical nanowire) is given by multiplication of the depolarization factor with  $E_{\text{out}\perp}$  as follows:<sup>40</sup>

$$E_{\text{in}\perp} = \frac{(2 \times E_{\text{out}\perp})}{1 + \epsilon(\omega)}$$

Polarization anisotropy ( $\rho$ ) is given by:<sup>40</sup>

$$\rho = \frac{|E_{\text{in}\parallel}|^2}{|E_{\text{in}\perp}|^2} = \frac{I_{\parallel}}{I_{\perp}} = \frac{|1 + \epsilon(\omega)|^2}{4}$$

From the angle dependent PL measurements in the normal direction (Fig. 3c), we obtain a polarization anisotropy of  $\rho = 5.7$  to  $10.8$ . This suggests that light emission characteristics can be modulated by an order of magnitude depending on the polarizing field direction with respect to the chain ( $b$ -axis) lattice direction. The polarization anisotropy of  $\text{ZrS}_3$  is smaller as compared to that of nanowires where  $\rho$  is in the range of  $20$ – $30$ .<sup>26,27</sup> This variation in polarization anisotropy can be partly justified by considering a much lower effective permittivity contrast  $\epsilon(\omega)_{\text{chain}}$  for a 1D chain embedded in a matrix of  $\text{ZrS}_3$  (Fig. 4b), as compared to a free-standing nanowire under vacuum

with a permittivity contrast of  $\epsilon(\omega)$  (Fig. 4a). Indeed, a similar reduction in  $\rho$  has been observed when luminescent nanowires ( $\text{ZnO}$ ,  $\text{InP}$ ) were coated with  $\text{Ta}_2\text{O}_5$ ,<sup>41</sup> surrounded by a matched dielectric medium, different from that observed under vacuum.

From a materials perspective, the reduction of the polarization anisotropy can be explained when one accounts for the interaction between adjacent pseudo-1D chains. A closer look at Fig. 4c shows that the PL intensity is relatively large at  $90^\circ$  even when the E-field is polarized across the chain ( $b$ -axis) direction and absorption is anticipated to be negligible as the E-field is greatly attenuated. A similar PL contribution can be seen in the orthogonal direction at  $0^\circ$  (Fig. 4b), and is responsible for reduced polarization anisotropy ( $I_{\parallel}/I_{\perp}$ ). Since 1D chains interact with each other, unlike suspended/non-interacting semiconducting nanowires, their optical response can be envisioned as a superposition of 2D planar (isotropic) and 1D chain-like (anisotropic) components. By simple geometrical considerations, chain-like PL intensity ( $I_{1D}$ ) scales as  $\cos^2$  which is essentially the same for 1D nanowires,  $I_{1D} = A \cos^2[(n \times \varphi) + x] + B_1$  ( $A$ ,  $n$ ,  $x$  and  $B_1$  are parameters). This function is represented by blue dashed lines in Fig. 4b and c, and is responsible for the observed anisotropy. Similar to  $\text{MoS}_2$  monolayers in Fig. 3b (red dotted data points), the 2D PL intensity ( $I_{2D}$ ) is represented by red dashed lines in Fig. 4b and c, and the superposition of  $I_{1D}$  and  $I_{2D}$  matches well with our experimental data (black solid line and green dots). Here, the fitting  $I_{1D}$  chain yields  $\rho = 27$  (as a fitting parameter), which is close to that observed in truly one dimensional systems. Overall, this 1D + 2D model accounts for the light emission characteristics in pseudo-1D materials.

## Conclusion

In summary, angle resolved PL spectroscopy measurements on  $\text{ZrS}_3$  few-layer flakes, density functional theory calculations, and electromagnetic theory based model are presented in

order to establish how the structural anisotropy of  $ZrS_3$  influences the optical properties of pseudo-1D transition metal trichalcogenide (TMTCs)  $ZrS_3$ . Our findings establish the nature of strong emission from  $ZrS_3$ , and also mark the very first demonstration of an anisotropic light emission response from TMTCs. Interestingly, polarization anisotropy of pseudo-1D  $ZrS_3$  appear smaller as compared to truly 1D nanowire/nanotube materials. Strong optical anisotropy and reduced polarization anisotropy is explained by a model based on electromagnetic theory which envisions the optics of quasi-1D materials as a superposition of the truly 1D and truly 2D optical response to account for the finite interaction between adjacent 1D chains. Overall findings not only contribute to the understanding of quasi-1D materials, particularly a new class of TMTCs, but also open new avenues for applications in biosciences and optical communication technologies where polarized light emission/absorption is essential for successful device operation.

## Computational methodology

We performed first-principles calculations which are carried out in the framework of density functional theory (DFT) as implemented in the Vienna *ab-initio* Simulation Package (VASP).<sup>43,44</sup> Generalized gradient approximation (GGA) of Perdew–Burke–Ernzerhof (PBE) was employed for the exchange and correlation potentials.<sup>45</sup> A  $20 \times 30 \times 11$   $\Gamma$ -centered  $k$ -point mesh was used for the Brillouin-zone (BZ) integration for the primitive unit cell of bulk  $ZrS_3$ . Frozen-core projector augmented wave (PAW) potentials are used with 500 eV kinetic energy cutoff for the plane-wave expansion.<sup>46</sup> The convergence criterion for energy is set to  $10^{-5}$  eV between two consecutive steps in the self-consistent field calculations. The atomic positions are relaxed until the Hellmann–Feynman forces are less than  $10^{-4}$  eV  $\text{\AA}^{-1}$ . In order to describe the van der Waals interaction between  $ZrS_3$  layers correctly, the DFT-D2 method of Grimme as implemented in VASP was used.<sup>47</sup> The screened-nonlocal-exchange Heyd–Scuseria–Ernzerhof (HSE) functional of the generalized Kohn–Sham scheme was used to obtain more accurate electronic structure calculations.<sup>48</sup>

## Acknowledgements

S. Tongay gratefully acknowledges support from NSF DMR-1552220. This work was supported by the Flemish Science Foundation (FWO-VI) and the Methusalem foundation of the Flemish government. Computational resources were provided by TUBITAK ULAKBIM, High Performance and Grid Computing Center (TR-Grid e-Infrastructure). HS is supported by a FWO postdoctoral fellowship.

## References

- 1 K. S. Novoselov, Electric Field Effect in Atomically Thin Carbon Films, *Science*, 2004, **306**(5696), 666–669.
- 2 A. H. Castro Neto, F. Guinea, N. M. R. Peres, K. S. Novoselov and A. K. Geim, The electronic properties of graphene, *Rev. Mod. Phys.*, 2009, **81**(1), 109–162.
- 3 A. K. Geim, Graphene: Status and Prospects, *Science*, 2009, **324**(5934), 1530–1534.
- 4 K. F. Mak, C. Lee, J. Hone, J. Shan and T. F. Heinz, Atomically thin  $MoS_2$ : A new direct-gap semiconductor, *Phys. Rev. Lett.*, 2010, **105**(13), 2–5.
- 5 A. Ramasubramaniam, Large excitonic effects in monolayers of molybdenum and tungsten dichalcogenides, *Phys. Rev. B: Condens. Matter Mater. Phys.*, 2012, **86**(11), 1–6.
- 6 Q. H. Wang, K. Kalantar-Zadeh, A. Kis, J. N. Coleman and M. S. Strano, Electronics and optoelectronics of two-dimensional transition metal dichalcogenides, *Nat. Nanotechnol.*, 2012, **7**(11), 699–712.
- 7 F. Xia, H. Wang and Y. Jia, Rediscovering black phosphorus as an anisotropic layered material for optoelectronics and electronics, *Nat. Commun.*, 2014, **5**, 4458.
- 8 D. J. Late, B. Liu, J. Luo, A. Yan, H. S. S. R. Matte, M. Grayson, C. N. R. Rao and V. P. Dravid, GaS and GaSe ultrathin layer transistors, *Adv. Mater.*, 2012, **24**(26), 3549–3554.
- 9 Y. Ma, Y. Dai, M. Guo, L. Yu and B. Huang, Tunable electronic and dielectric behavior of GaS and GaSe monolayers, *Phys. Chem. Chem. Phys.*, 2013, **15**(19), 7098–7105.
- 10 D. Wickramaratne, F. Zahid and R. K. Lake, Electronic and thermoelectric properties of van der Waals materials with ring-shaped valence bands, *J. Appl. Phys.*, 2015, **118**(7), 075101.
- 11 O. B. Aslan, D. A. Chenet, A. M. Van der Zande, J. C. Hone and T. F. Heinz, Linearly Polarized Excitons in Single- and Few-Layer  $ReS_2$  Crystals, *ACS Photonics*, 2016, **3**(1), 96–101.
- 12 Y. C. Lin, H. P. Komsa, C. H. Yeh, T. Björkman, Z. Y. Liang, C. H. Ho, Y. S. Huang, P. W. Chiu, A. V. Krasheninnikov and K. Suenaga, Single-Layer  $ReS_2$ : Two-Dimensional Semiconductor with Tunable In-Plane Anisotropy, *ACS Nano*, 2015, **9**(11), 11249–11257.
- 13 J. Qiao, X. Kong, Z.-X. Hu, F. Yang and W. Ji, High-mobility transport anisotropy and linear dichroism in few-layer black phosphorus, *Nat. Commun.*, 2014, **5**, 4475.
- 14 H. Liu, A. T. Neal, Z. Zhu, Z. Luo, X. Xu, D. Tománek and P. D. Ye, Phosphorene: An unexplored 2D semiconductor with a high hole mobility, *ACS Nano*, 2014, **8**(4), 4033–4041.
- 15 Y. Jin, X. Li and J. Yang, Single layer of  $MX_3$  ( $M = Ti, Zr; X = S, Se, Te$ ): a new platform for nano-electronics and optics, *Phys. Chem. Chem. Phys.*, 2015, **17**(28), 18665–18669.
- 16 M. Pacilé, D. Papagno, M. Lavagnini, M. Berger, H. Degiorgi and L. Grioni, Photoemission and optical studies of  $ZrSe_3$ ,  $HfSe_3$ , and  $ZrS_3$ , *Phys. Rev. B: Condens. Matter Mater. Phys.*, 2007, **76**(15), 1–8.
- 17 J. Kang, H. Sahin, H. D. Ozaydin, R. T. Senger and F. M. Peeters,  $TiS_3$  nanoribbons: Width-independent band gap and strain-tunable electronic properties, *Phys. Rev. B: Condens. Matter*, 2015, **92**(7), 075413.
- 18 J. Kang, H. Sahin and F. M. Peeters, Mechanical Properties of Monolayer Sulphides: A Comparative Study between  $MoS_2$ ,  $HfS_2$  and  $TiS_3$ , *Phys. Chem. Chem. Phys.*, 2015, 42–45.

- 19 F. Iyikanat, H. Sahin, R. T. Senger and F. M. Peeters, Vacancy Formation and Oxidation Characteristics of Single Layer  $\text{TiS}_3$ , *J. Phys. Chem. C*, 2015, **119**(19), 10709–10715.
- 20 J. O. Island, R. Biele, M. Barawi, J. M. Clamagirand, J. R. Ares, C. Sánchez, H. S. J. Van Der Zant, I. J. Ferrer, R. D. Agosta and A. Castellanos-gomez, Titanium trisulfide ( $\text{TiS}_3$ ): a 2D semiconductor with quasi-1D optical and electronic properties, *Sci. Rep.*, 2016, **6**, 22214.
- 21 V. Tran, R. Soklaski, Y. Liang and L. Yang, Layer-controlled band gap and anisotropic excitons in few-layer black phosphorus, *Phys. Rev. B: Condens. Matter*, 2014, **89**(23), 235319.
- 22 S. Tongay, H. Sahin, C. Ko, A. Luce, W. Fan, K. Liu, J. Zhou, Y.-S. Huang, C.-H. Ho, J. Yan, D. F. Ogletree, S. Aloni, J. Ji, S. Li, J. Li, F. M. Peeters and J. Wu, Monolayer behaviour in bulk  $\text{ReS}_2$  due to electronic and vibrational decoupling, *Nat. Commun.*, 2014, **5**, 3252.
- 23 F. Liu, S. Zheng, X. He, A. Chaturvedi, J. He, W. L. Chow, T. R. Mion, X. Wang, J. Zhou, Q. Fu, H. J. Fan, B. K. Tay, L. Song, R.-H. He, C. Kloc, P. M. Ajayan and Z. Liu, Highly Sensitive Detection of Polarized Light Using Anisotropic 2D  $\text{ReS}_2$ , *Adv. Funct. Mater.*, 2016, **26**(8), 1169–1177.
- 24 X. Wang, A. M. Jones, K. L. Seyler, V. Tran, Y. Jia, H. Zhao, H. Wang, L. Yang, X. Xu and F. Xia, Highly anisotropic and robust excitons in monolayer black phosphorus, *Nat. Nanotechnol.*, 2015, **10**(6), 517–521.
- 25 A. Ait-Ouali and S. Jandl, Two-dimensional indirect excitons in the layer-type trichalcogenide  $\text{ZrS}_3$ , *Phys. Rev. B: Condens. Matter*, 1994, **49**(3), 1813–1817.
- 26 T. M. Rümke, J. A. Sánchez-Gil, O. L. Muskens, M. T. Borgström, E. P. Bakkers and J. Gómez Rivas, Local and anisotropic excitation of surface plasmon polaritons by semiconductor nanowires, *Opt. Express*, 2008, **16**(7), 5013.
- 27 J. Wang, Highly Polarized Photoluminescence and Photodetection from Single Indium Phosphide Nanowires, *Science*, 2001, **293**(5534), 1455–1457.
- 28 T. Wieting, A. Grisel, F. Levy and P. Schmid, Quasi-One-Dimensional Conductors I, *Lect. Notes Phys.*, 1979, **95**, 354.
- 29 Y.-R. Tao, J.-J. Wu and X.-C. Wu, Enhanced ultraviolet-visible light responses of phototransistors based on single and a few  $\text{ZrS}_3$  nanobelts, *Nanoscale*, 2015, **7**(34), 14292–14298.
- 30 H. Jin, D. Cheng, J. Li, X. Cao, B. Li, X. Wang, X. Liu and X. Zhao, Facile synthesis of zirconium trisulfide and hafnium trisulfide nanobelts: Growth mechanism and Raman spectroscopy, *Solid State Sci.*, 2011, **13**(5), 1166–1171.
- 31 L. Huang, K. Tang, Q. Yang, G. Shen and S. Jia, Synthesis and characterization of  $\text{ZrS}_3$  nanocrystallites, *Mater. Res. Bull.*, 2004, **39**(7–8), 1083–1089.
- 32 C. Sourisseau and Y. Mathey, The infrared, Raman, resonance Raman spectra and the valence force field of the  $\text{ZrS}_3$  Tightly Bound Triions in Transition Metal Dichalcogenide Hetero-structures layer-type compound, *Chem. Phys.*, 1981, **63**(1–2), 143–156.
- 33 J. Heyd, G. E. Scuseria and M. Ernzerhof, Hybrid functionals based on a screened Coulomb potential, *J. Chem. Phys.*, 2003, **118**(18), 8207–8215.
- 34 Y. Zhang, B. Fluegel, A. Mascarenhas, H. Xin and C. Tu, Optical transitions in the isoelectronically doped semiconductor  $\text{GaP:N}$ : An evolution from isolated centers, pairs, and clusters to an impurity band, *Phys. Rev. B: Condens. Matter*, 2000, **62**(7), 4493–4500.
- 35 G. D. Gilliland, Photoluminescence spectroscopy of crystalline semiconductors, *Mater. Sci. Eng., R*, 1997, **18**(3–6), 99–399.
- 36 M. Z. Bellus, F. Ceballos, H. Chiu and H. Zhao, Tightly Bound Triions in Transition Metal Dichalcogenide Heterostructures, *ACS Nano*, 2015, **9**(6), 6459–6464.
- 37 A. R. Klots, A. K. M. Newaz, B. Wang, D. Prasai, H. Krzyzanowska, D. Caudel, N. J. Ghimire, J. Yan, B. L. Ivanov, K. A. Velizhanin, A. Burger, D. G. Mandrus, N. H. Tolk, S. T. Pantelides and K. I. Bolotin, Probing excitonic states in ultraclean suspended two-dimensional semiconductors by photocurrent spectroscopy, *Sci. Rep.*, 2014, **4**, 6608.
- 38 S. Tongay, J. Suh, C. Ataca, W. Fan, A. Luce, J. S. Kang, J. Liu, C. Ko, R. Raghunathanan, J. Zhou, F. Ogletree, J. Li, J. C. Grossman and J. Wu, Defects activated photoluminescence in two-dimensional semiconductors: interplay between bound, charged, and free excitons., *Sci. Rep.*, 2013, **3**, 2657.
- 39 A. Ait-Ouali and S. Jandl, Photoluminescence study of the one-dimensional material  $\text{ZrS}_3$  and its solid solution  $\text{Zr}_{1-x}\text{Hf}_x\text{S}_3$ , *Phys. Rev. B: Condens. Matter*, 1996, **53**(15), 9852–9858.
- 40 J. G. Rivas, O. L. Muskens, M. T. Borgström, S. L. Diedenhofen and E. P. A. M. Bakkers, Optical Anisotropy of Semiconductor Nanowires, in *One-Dimensional Nanostructures*, ed. Z. M. Wang, Springer New York, New York, NY, 2008, pp. 127–145.
- 41 L. Fang, X. Zhao, Y.-H. Chiu, D. Ko, K. M. Reddy, T. R. Lemberger, N. P. Padture, F. Yang and E. Johnston-Halperin, Comprehensive control of optical polarization anisotropy in semiconducting nanowires, *Appl. Phys. Lett.*, 2011, **99**(14), 141101.
- 42 K. Wu, B. Chen, S. Yang, G. Wang, W. Kong, H. Cai, T. Aoki, E. Soignard, X. Marie, A. Yano, A. Suslu, B. Urbaszek and S. Tongay, Domain architectures and grain boundaries in chemical vapor deposited highly anisotropic  $\text{ReS}_2$  monolayer films, *Nano Lett.*, 2016, DOI: 10.1021/acs.nanolett.6b02766.
- 43 G. Kresse and J. Furthmüller, Efficiency of *ab-initio* total energy calculations for metals and semiconductors using a plane-wave basis set, *Comput. Mater. Sci.*, 1996, **6**, 15–50.
- 44 G. Kresse and J. Furthmüller, Efficient iterative schemes for *ab initio* total-energy calculations using a plane-wave basis set, *Phys. Rev. B*, 1996, **54**, 11169–11186.
- 45 J. P. Perdew, K. Burke and M. Ernzerhof, Generalized gradient approximation made simple, *Phys. Rev. Lett.*, 1996, **77**, 3865–3868.
- 46 P. E. Blöchl, Projector augmented-wave method, *Phys. Rev. B*, 1994, **50**, 17953–17979.
- 47 S. Grimme, Semiempirical GGA-type density functional constructed with a long-range dispersion correction, *J. Comput. Chem.*, 2006, **27**, 1787–1799.
- 48 J. Heyd, G. E. Scuseria and M. Ernzerhof, Hybrid functionals based on a screened Coulomb potential, *J. Chem. Phys.*, 2003, **118**, 8207.